JOC The Journal of Organic Chemistry

Article

Inhibitory and Cooperative Effects Regulated by pH in Host-Guest Complexation Between Cationic Pillar[5]arene and Reactive 2-Carboxyphthalanilic Acid

Eduardo V. Silveira, Vanessa Nascimento, Eduardo H. Wanderlind, Ricardo Ferreira Affeldt, Gustavo Amadeu Micke, Luis García#Río, and Faruk Nome

J. Org. Chem., **Just Accepted Manuscript** • DOI: 10.1021/acs.joc.9b01377 • Publication Date (Web): 08 Jul 2019

Just Accepted

is published by the American Chemical Society. 1155 Sixteenth Street N.W., Washington, DC 20036

Inhibitory and Cooperative Effects Regulated by pH in Host-Guest Complexation Between Cationic Pillar[5]arene and Reactive 2-Carboxyphthalanilic Acid

Eduardo V. Silveira,*[,†] Vanessa Nascimento,[††] Eduardo H. Wanderlind,[†] Ricardo F. Affeldt,*[,†] Gustavo A. Micke,[†] Luis Garcia-Rio, [†††] and Faruk Nome[†,¶]

[†]Departamento de Química, Universidade Federal de Santa Catarina, Florianópolis – SC, 88040-900, Brazil.

[††]Departamento de Química Orgânica, Universidade Federal Fluminense, Niterói – RJ, 24020-150, Brazil.

[†††]Centro de Investigación en Química Biolóxica e Materiais Moleculares (CiQUS), Departamento de Química Física, Universidade de Santiago de Compostela, 15782, Santiago de Compostela, Spain.

*eduardoifg@hotmail.com; ricardo.affeldt@ufsc.br

KEYWORDS: *Pillararene, host-guest, inhibition, allosteric, spatiotemporal, amide decomposition*

ABSTRACT: The study of host-guest complexation between reactive 2-carboxyphthalanilic acid (CPA) and two cationic pillararenes has been carried out. Host-guest complexation with significant kinetic effects were observed only with the smaller cavity size pillararene (P5A). Kinetics in the pH-range 1.50-6.40, ESI-MS, ^{1}H NMR titration and ROESY experiments were performed to characterize the complexes. High binding stoichiometry (H:G_2) was observed for all CPA protonation states. The system is pH-dependent and inversion of cooperativity (negative to positive) occurs by increasing the dianionic CPA^{2-} concentration (allosteric behavior). Towards physiological pH, association constant $K_{1:1}$ does not change (10^4 M^{-1}) and $K_{1:2}$ increased from 10^2 to 10^4 M^{-1}, as well as the inhibitory effect increase up to 222-fold. NMR results elucidated the structure of the complex and allowed us to create a map of H-H interactions that describes well the diversity and number of interactions in the complex.

INTRODUCTION

Since 2008 and still considered a recent class of macrocycles,[1] the pillararenes are widely used in several areas,[2–5] mainly in catalysis and in the development of chemical sensors.[6–9] Its use in the inhibition of organic reactions is a less common practice, such as found for other types of host,[10–13] where the aim is to reduce the rate of reaction or reactivity of some species. As in catalytic systems, inhibitory systems are also able to provide very important information about the components (host and guest), alone or as complex, being the information extracted by the simple relationship between environment and reactivity.

Very important applications can rise from the inhibition of organic reactions. For example, the action of acetylcholinesterase on acetylcholine was inhibited by the host-guest association of the neurotransmitter with an anionic pillar[5]arene, a model system for the treatment of Alzheimer's disease.[14] In another work,[15] a cationic pillar[6]arene incorporated into micelles proved to be efficient in targeting into cancer cells (via folate receptors), forming a host-guest complex with intracellular ATP (adenosine-5'-triphosphate) inhibiting its hydrolysis. Suppression of this energy source resulted in the blockade of the efflux pump and reduced the elimination of chemotherapeutic drugs (such as doxorrubicin), potentiating anticancer treatment.

Moravetz *et. al*. have demonstrated the intramolecular reactivity of 2-carboxyphthalanic acid (CPA) as a bifunctional intramolecular catalysis model (Scheme 1).[16] A perspective of this catalytic effect in terms of the spatiotemporal theory is able to provide a better understanding of the high enzymatic efficiency, such as in aspartic proteases (accelerations up to 10^{10}-fold).[17] Similarly, the enzymatic inhibition can be understood in the same way, that is, reduction of the catalytic efficiency by the steric restriction of its catalytic groups. These considerations make the CPA reactivity an excellent model reaction for this study.

Inhibition on CPA decomposition is mainly based on the restriction of its two carboxyl groups. The concepts of unfavorable position (spatio) and length time (temporal) can also be applied to different types of intramolecular reactions, such as decomposition[18] and cyclization[19]. This strategy is of great interest when one seeks to keep intact the properties and functionalities of a particular species in a reactive environment, a concept that can be extended to several areas, such as synthesis and drug delivery.[20,21]

Scheme 1. Acid dissociation equilibria of CPA and its decomposition, based on the literature.[16]

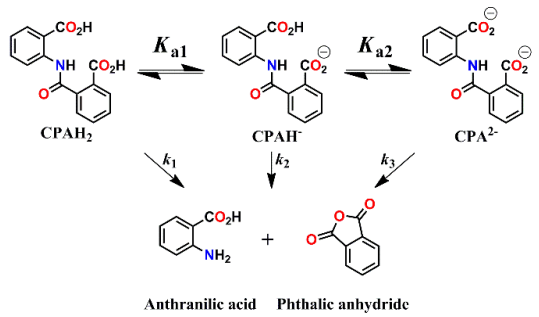

Herein, we investigate the host-guest complex between two cationic pillararenes (P5A and P6A) and CPA (Chart 1). The pillararene with smaller cavity size (P5A) proved to be a highly selective host with inhibitory kinetic effects on CPA decomposition. We performed a complete study about the influence of pH on the kinetic and equilibrium parameters of the system. Through different techniques (UV-Vis, ESI-MS and NMR) we determined rate and association constants, cooperativity effects, stoichiometry and structural elucidation of the complex. From the ^{1}H NMR data (titration and ROESY) we created a "map of H-H interactions" of the complex, making clear the great diversity and number of interactions in the system. The properties of the investigated system make it a good model for development of pH- and environment-dependent inhibitors.

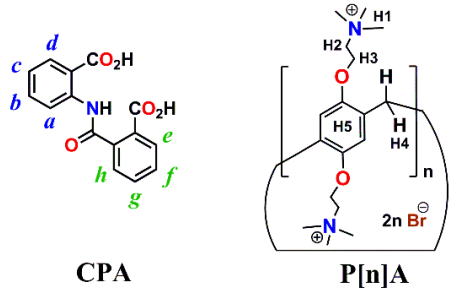

Chart 1. Structures of hosts (P5A and P6A) and guest (2-carboxyphthalanic acid, CPA).

RESULTS AND DISCUSSION

Kinetics. After elucidating the decomposition products of CPA (Scheme 1 and SI), we studied its decomposition in the presence of P5A and P6A in the pH-range of 1.50–6.40. Insignificant inhibitory kinetic effects (2.5-fold) occurred with P6A, while P5A caused high inhibition of the reaction. Figure 1A shows the pH-rate profiles of the spontaneous hydrolysis of CPA (black data) and in the presence of P5A (green data), with clear effects of inhibition towards the physiological pH. Errors were avoided by using concentrations of P5A suffice to ensure complexation of all CPA.

The data fitting in Figure 1A (Equation S1) provided the pK_a values of CPA in both water (pK_{a1}^{w} and pK_{a2}^{w}) and in the P5A cavity (pK_{a1}^{P5A} and pK_{a2}^{P5A}), occurring reduction of almost 1 unit after complexation. This increase in the acidity of the CPA is a result of the electrostatic stabilization promoted by the NMe_3^+ groups on its carboxyl groups, reaching ΔpK_{a1} = -0.62 and ΔpK_{a2} = -0.77. Therefore, the relative fractions of the neutral CPA ($CPAH_2$), monoanionic ($CPAH^-$) and dianionic (CPA^{2-}) species were calculated in water and in the P5A cavity as a function of pH (Figure 1B), with the approximation between pK_{a1}^{P5A} and pK_{a2}^{P5A} responsible for the reduction of 4.2 % of the $CPAH^-$ species (represented by the red arrow).

At this point the experimental data suggest that: (1) the complex is pH-dependent; (2) the inhibitory effect of the reaction increases with pH and (3) the high electrostatic stabilization on the anionic CPA should result in increasing association constants in the order of $CPAH_2 < CPAH^- < CPA^{2-}$.

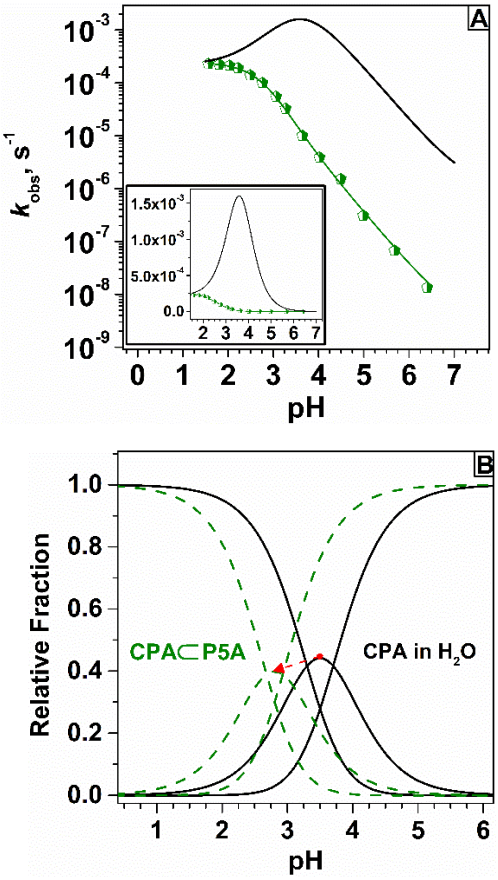

Figure 1. (A) Influence of pH on the first-order rate constant for CPA spontaneous hydrolysis (black data) and in the P5A cavity (green data), at 25.0 ºC ([CPA] = 1.0×10^{-4} M; [P5A] = 4.0×10^{-4} M). (B) Relative percentages of the CPA species in H_2O (black solid lines) and in the P5A cavity (green dashed lines) as a function of pH.

The influence of the P5A concentration on the k_{obs} for CPA^{2-} decomposition was directly determined by kinetic experiments at pH 6.00 (Figure 2A and Table 1). The stoichiometric analysis by fitting data (Equations S2-S3) revealed the typical behavior of a H:G_2 system with a strong positive cooperativity (α = 10.9, calculated by $\alpha = 4K_{1:2}/K_{1:1}$), indicating the modification of the P5A cavity after binding of the first CPA^{2-}. In other words, the $CPA^{2-}\subset$P5A offers a more favorable binding site than the free P5A, and the difference between the free energy variations

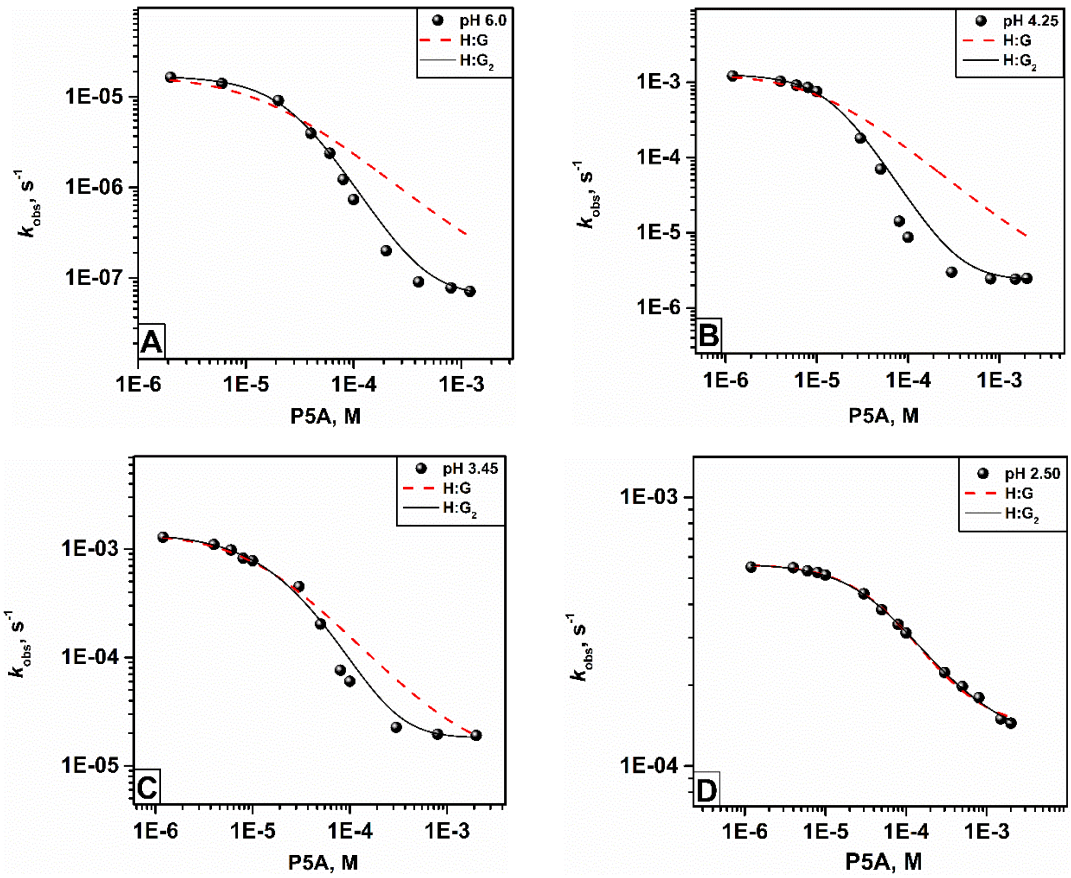

Figure 2. Influence of P5A concentration on the k_{obs} for CPA decomposition at pHs (A) 6.00, (B) 4.25, (C) 3.45 and (D) 2.50 ([CPA] = 1.0 × 10^{-4} M; 25.0 ºC).

Table 1. Rate and equilibrium constants to CPA in P5A cavity at pHs 2.50, 3.45, 4.25 and 6.00.

pH	$k_{1:1}$ (s^{-1})	$k_{1:2}$ (s^{-1})	$K_{1:1}$ (10^4, M^{-1})	$K_{1:2}$ (M^{-1})	K_G (M^{-2})
2.50	(1.87 ± 0.1) × 10^{-4}	(1.21 ± 0.1) × 10^{-4}	(1.69 ± 0.4) × 10^4	(997 ± 478)	1.68 × 10^7
3.45	(1.16 ± 3.5) × 10^{-5}	(1.82 ± 2.3) × 10^{-5}	(7.15 ± 1.1) × 10^4	(1.29 ± 2.4) × 10^4	9.22 × 10^8
4.25	(1.81 ± 7.1) × 10^{-5}	(2.30 ± 11.1) × 10^{-6}	(3.58 ± 0.8) × 10^4	(1.31 ± 0.6) × 10^5	4.69 × 10^9
6.00	(1.50 ± 8.3) × 10^{-7}	(6.31 ± 15.4) × 10^{-8}	(2.29 ± 0.5) × 10^4 [(a)]	(6.22 ± 2.6) × 10^4 [(b)]	1.42 × 10^9

of the subsequent associations gives us a quantitative energy analysis, such as $\Delta\Delta G = \Delta G_{1:2} - \Delta G_{1:1}$ = -2.48 kJ·mol^{-1} (see Table 2). The obtained rate constants remained in the order of $k_{1:1}{}^{D} = 10^{-7}$ s^{-1} and $k_{1:2}{}^{D} = 10^{-8}$ s^{-1}, magnitudes compatible with the data of Figure 1A.

For the other species ($CPAH_2$ and $CPAH^-$) the direct determination of its parameters was difficult due to the complexity of the system considering the distribution of all species in both environments (H_2O and P5A) and possible changes of stoichiometry. Therefore, we investigated the influence of P5A concentration on the k_{obs} at pHs 2.50, 3.45 and 4.25 (Figures 2B-C and Table 1) to evaluate the stoichiometry, cooperativity and association constants to compare with values obtained by the thermodynamic cycle (Scheme 2), as shown later. Thus, we emphasize that the data at these pHs should not be attributed to a single species or species distribution due to variation with increasing P5A concentration. The maximum and minimum fractions of each species were calculated for theses pHs in both environments and are shown in Table S3.

The data fitting at pH 2.50 were satisfactory for both H:G and H:G_2 stoichiometries (Figure 2D). However, the predominance of $CPAH_2$ in both environments (H_2O = 85.5 % and P5A = 52.5 %) and the association constants obtained for H:G (1.43 × 10^4 M^{-1}) and H:G_2 global ($K_G = K_{1:1} \times K_{1:2}$ = 1.68 × 10^7 M^{-2}) indicate the system as H:G_2. This conclusion was made after we obtained the same magnitude of K_G to $CPAH_2$ through calculations involving the thermodynamic

Scheme 2. Acid dissociation equilibria of CPA (in water and in the P5A cavity) and association equilibria of all species with P5A (stepwise for CPA^{2-} and global for $CPAH_2$ and $CPAH^-$).

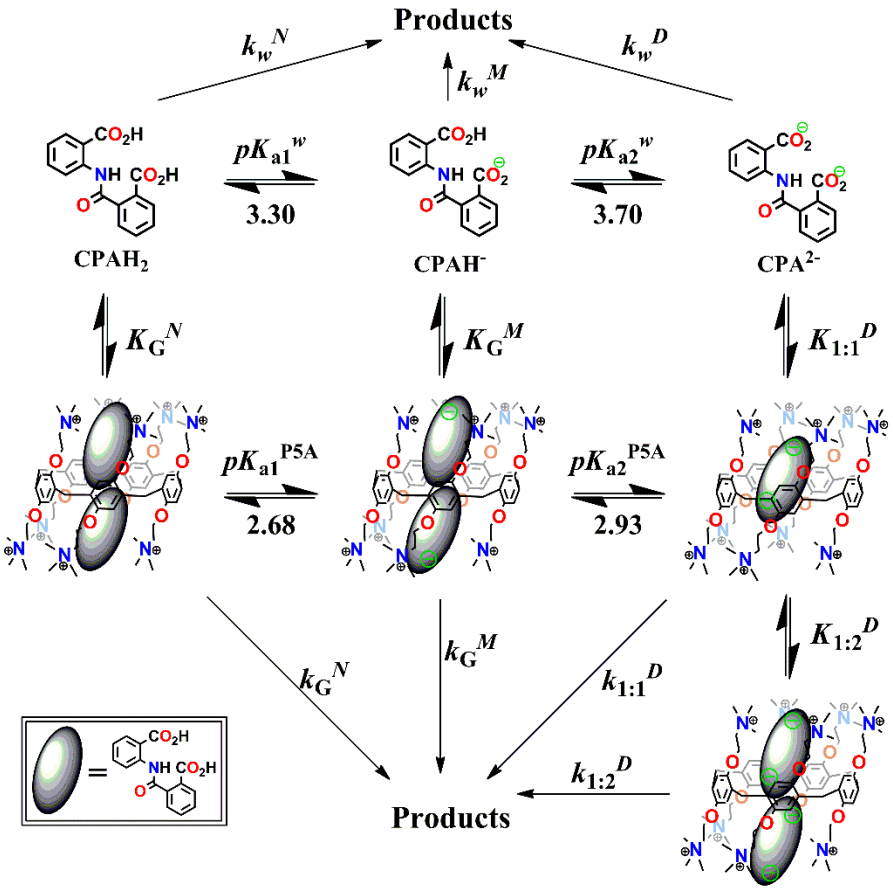

cycle. Another important observation is the negative cooperativity at this pH (α = 0.24), an effect that must be mainly influenced by $CPAH_2$ species.

For the other pHs the data fitting was satisfactory only as H:G_2 (Figures 2B-C) to give values of $K_G^{pH\_3.45} = 10^8$ M^{-2} and $K_G^{pH\_4.25} = 10^9$ M^{-2}, magnitudes also similar to those obtained to $CPAH^-$ (by the cycle) and CPA^{2-} (directly at pH 6.00), respectively. In these pHs, the cooperativity ($\alpha^{pH\_3.45} = 0.72$ and $\alpha^{pH\_4.25} = 14.63$) and the molar fractions of each species in both environments (Table S3) show the inversion of cooperativity (negative to positive) when [$CPAH_2$] << [CPA^{2-}], that is, positive cooperativity is promoted by the dianionic species. Standard errors in data fitting increase with pH and are more expressive at pH 6.00. This suggests that the errors are not related to the variation of the relative fractions after increasing P5A concentration, but with the modification of pK_{a1}^{P5A} and pK_{a2}^{P5A} after binding of the first CPA in the P5A cavity. This is a result of interactions between CPAs within the P5A cavity and increases with its ionization, that is, in the order of $CPAH^-$ < CPA^{2-}. The rate constants in the P5A cavity also have a good relationship with the data of Figure 1A.

Table 1 allows us to make two important considerations. First, the magnitude of $K_{1:1} = 10^4$ M^{-1} for all pHs suggests non-electrostatic interactions as the main driving force involved in the binding of the first CPA, such as hydrophobic effects and involving the π systems (cation-π, π-π and CH-π). Second, the inversion of cooperativity is dependent of the CPA^{2-} concentration, indicating that the electrostatic interaction favors the accommodation of the second CPA into the cavity of P5A. This behavior is similar to that of allosteric enzymes (regulation of metabolism) and shows intelligence in response to pH.[22–24] These considerations led us to the elaboration of Scheme 2, considering the global behavior (kinetic and equilibrium) for $CPAH_2$ and $CPAH^-$ and stepwise for the CPA^{2-}.

We consider that binding of the first CPA does not modify pK_{a1}^{P5A} and pK_{a2}^{P5A} and we calculated the K_G^N and K_G^M by the thermodynamic cycle (Scheme 2). For this, we replaced K_G^D and pK_a values in Equations 1-2 and obtained values with similar magnitudes to those determined above at different pHs (10^7–10^9 M^{-2}). For these species, the global or apparent rate constants (k_G) in the P5A cavity were extracted from the data fitting of Figure 1A (green data), all presented in Table 2.

$$K_G^D = K_G^M \frac{K_{a2}^{P5A}}{K_{a2}^w} \quad (1) \qquad K_G^M = K_G^N \frac{K_{a1}^{P5A}}{K_{a1}^w} \quad (2)$$

K_G^D, K_G^M and K_G^N are the global association constants of the species CPA^{2-} (obtained at pH 6.00), $CPAH^-$ and $CPAH_2$, respectively; K_{a1}^w and K_{a2}^w are the acidity constants of the CPA in water; K_{a1}^{P5A} and K_{a2}^{P5A} are the acidity constants of the CPA in P5A cavity.

Table 2. Rate and equilibrium constants to CPA species in H_2O and P5A cavity.

Species	k_w (s^{-1})	$k_{1:1}$ (s^{-1})	$k_{1:2}$ (s^{-1})	$K_{1:1}$ (M^{-1})	$K_{1:2}$ (M^{-1})
$CPAH_2$	2.1×10^{-4}	$k_G^N = 2.37 \times 10^{-4}$		$K_G^N = 5.81 \times 10^7\ M^{-2}$	
$CPAH^-$	4.0×10^{-3}	$k_G^M = 4.10 \times 10^{-5}$		$K_G^M = 2.42 \times 10^8\ M^{-2}$	
CPA^{2-}	1.4×10^{-5}	$(1.50 \pm 8.3) \times 10^{-7}$	$(6.31 \pm 15.4) \times 10^{-8}$	$(2.29 \pm 0.5) \times 10^{4}$ [a]	$(6.22 \pm 2.6) \times 10^{4}$ [b]
		$pK_{a1}^w = 3.30$; $pK_{a2}^w = 3.70$		$pK_{a1}^{P5A} = 2.68$; $pK_{a2}^{P5A} = 2.93$	

[a]ΔG = -24.88 kJ·mol^{-1}; [b]ΔG = -27.36 kJ·mol^{-1} (calculated by $\Delta G = -R \cdot T \cdot \ln K$).

Without the electrostatic component, $CPAH_2$ binds strongly in the hydrophobic cavity of P5A in H:G_2 system. This behavior is similar to that of nonpolar substrates associating in favorable geometries for water exclusion,[25] that is, hydrophobic associations. Other types of interactions are also predicted for this system and will be elucidated in the NMR topic.

The inhibitory effect on CPA decomposition is also very well explained by spatiotemporal theory.[26] The absence of the bell-shaped pH-rate profile in the presence of P5A (Figure 1A) clearly shows this effect, with the restriction of its carboxyl groups being the cause of this. First, we must consider that the proximity between pK_{a1}^{P5A} and pK_{a2}^{P5A} reduces 4.2 % of the $CPAH^-$, the main catalytic species. According to theory, the favorable position (distance and angle) for the carboxyl groups (spatio) and its length time (temporal) should be strongly impaired in the $CPAH^-$⊂P5A⊃$CPAH^-$ system. We also highlight that, in addition to the steric restriction of the carboxyl groups in the H:G_2 system, the NMe_3^+ groups should also contribute to this by electrostatic interactions.

ESI-MS. The characterization of P5A and CPA⊂P5A⊃CPA was performed by direct infusion in an ESI-MS spectrometer (Figure 3). Infusion of an aqueous solution of P5A (~10.0 μM) resulted in 8 *m/z* signals corresponding to the different combinations of P5A and its Br^- counterions (Figure 3A). The only unobserved signals were the smaller ionization species (P5A–1Br) and, of course, the neutral species (P5A–0Br).

The infusion of an equimolar aqueous solution of CPA and P5A (~10.0 μM) provided several signals corresponding to the combinations between CPA, P5A and Br^-, both in H:G and H:G_2 stoichiometries (Figure 3B). A complementary MS^2 study was performed on the signal of highest intensity (*m/z* = 324.0 Da) to confirm the structure of the complex (Figure 3C). The MS^2 spectrum, corresponding to the $[H:G_2–7Br]^{7+}$ fragmentation, provided signals indicating the loss of remaining Br^- (*m/z* = 186.8 Da), loss of Br^- and one of the CPAs (*m/z* = 175.9 Da), the anthranilic acid as the CPA fragment (*m/z* = 138.2 Da) and propadienyl radical as the common benzene fragment (*m/z* = 39.0 Da).

NMR. After identifying all CPA protons (Figure S6), ^{1}H NMR experiments (titration and ROESY) at pD 7.0 were performed to confirm stoichiometry, cooperativity, magnitude of K_G^D and elucidate the structure of the complex.

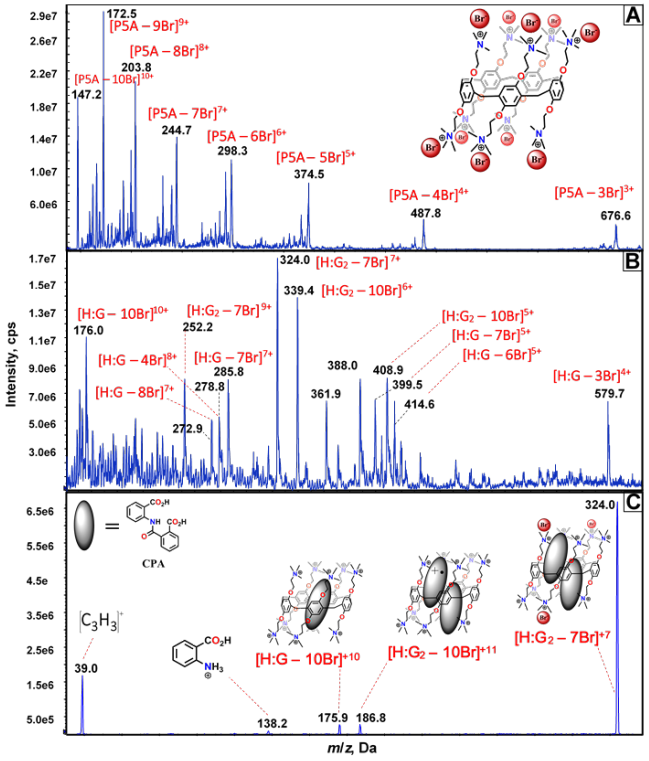

Figure 3. Full scan ESI-MS spectra in positive ion mode of aqueous solutions of (A) P5A, (B) equimolar CPA and P5A and (C) MS^2 of *m/z* = 324.0 Da of panel B (all compounds at ~10 μM).

Due to the low solubility of CPA, the addition of organic solvent (reduction of the hydrophobic effect) and the use of high concentrations of pillararenes (greater interference by Br^-) modified the conditions used in the kinetics, however, relevant qualitative information could be made.

For P6A, the ^{1}H NMR titration showed slight variations for all CPA protons with its binding isotherms presenting inaccurate profile. This behavior together with no significant kinetic effects suggests the formation of aggregates external to the macrocycle cavity (more details in SI). With the P5A distinct behavior was observed for the CPA^{2-} protons (Figure 4 and SI). All protons derived from phthalic anhydride (green protons) showed small downfield shift ($\Delta\delta$ = 0.062 ppm), probably due to its proximity to electronegative or positively charged groups, such as R-O-R and NMe_3^+ of P5A. Protons

derived from anthranilic acid (blue protons) showed strong upfield shift in the order of H*c* >> H*b* > H*d* ≅ H*a*, indicating its accommodation in the region of greater magnetic shielding in the P5A cavity. We emphasize that all P5A protons also showed upfield shift when in the complex, however, no plateau was reached, as in CPA^{2-}. This continuous deshielding may be a result of the association of Br^- with increasing P5A concentration, as already evidenced for other anionic counterions.[27] Another important observation is the splitting of some protons in the order of H*c* >> H*2* >> H*3* > H*b* (singlet to doublet, see SI), indicating an asymmetric accommodation of the CPAs in the P5A cavity.

For example, the Δδ *vs*. [P5A] for "H*c*" proton shows a slightly sigmoidal profile with satisfactory fitting data only as H:G_2 (Figure 5A; fitted to Equations S4-S5). Data fitting of all CPA protons provided $K_{1:2} = 10^4$–10^5 M^{-1}, $K_{1:1} < 1$ and $\delta_{1:1} < 0$ (see Table S4), these last two not having physical sense. Similar behaviors have already been reported in ^{1}H NMR titration when $K_{1:1} << K_{1:2}$, where an exemplified discussion demonstrates the impossibility of unequivocally determining stepwise association constants.[28] However, even with small errors in the fitting a qualitative analysis can be performed.

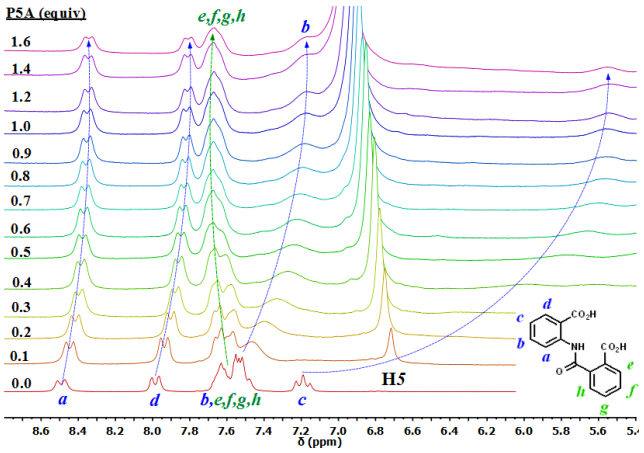

Figure 4. ^{1}H NMR spectra of CPA (31.87 mM) with different P5A equivalents (D_2O:MeOD, 1:1; pD 7.0; Bis-Tris methane 0.01 M; 25.0 ºC; 200 MHz).

Comparing with the kinetic data, the significant reduction of $K_{1:1}$ and the conservation of $K_{1:2}$ suggests hydrophobic interactions as the main driving force involved in the association of the first CPA^{2-}. Meanwhile $K_{1:2}$ must strongly depend on interactions within the P5A cavity. These evidences yield the increase in the positive cooperativity effect, making CPA^{2-}⊂P5A a more selective host for the second CPA^{2-}. This may also suggest that in a highly hydrophobic environment, such as cell membranes, the system delivers the CPAs due to the high destabilization of the complex.

Figure 5B shows the tangent method applied on the Δδ *vs*. $[P5A]_0/[CPA]_0$, and the inflection point of 0.5 confirm the H:G_2 binding stoichiometry. Commonly, a maximum of *x*(Host) = 0.33 is expected in Job's plot for H:G_2 system and different values certainly cause confusion. However, several factors influence the shape and the maximum value in Job's plot, such as host concentration, ratio of $K_{1:2}/K_{1:1}$ and the spectral variations of the complexes ($\delta_{1:1}$ and $\delta_{1:2}$). As demonstrated,[29] an H:G_2 system with common conditions ($[H]_0$ = 0.01 M; $K_{1:1}$ = 1,000 M^{-1}; $K_{1:2}$ = 250 M^{-1}; $\delta_{1:1}$ = 0 and $\delta_{1:2}$ = 1) reduce the maximum in Job's plot to *x*(Host) = 0.29. The maximum of *x*(P5A) = 0.21 in our Job's plot (insert on Figure 5B) represents the most pronounced effect of the influencing factors, corroborating with our experimental conditions (high P5A concentrations) and equilibrium parameters ($K_{1:1} << K_{1:2}$).

The ^{1}H ROESY study was performed to obtain structural information of the complex, a useful technique to determine the proximity between protons in intermolecular interactions. The partial spectrum (Figure 6, left) shows 14 cross-peaks corresponding to the CPA^{2-}--P5A and CPA^{2-}--CPA^{2-} interactions, with their intensities proportional to the distance between the nuclei. The aromatic protons of P5A (H*5*) present cross-peaks with protons derived from both CPA^{2-} aromatic rings (11, 12, 13 and 14), suggesting an antiparallel accommodation of CPAs in the P5A cavity. The cross-peak 10 confirms this (between H*c* and green protons) and corroborates with the splitting of protons, meaning the asymmetrical accommodation of the two guests.

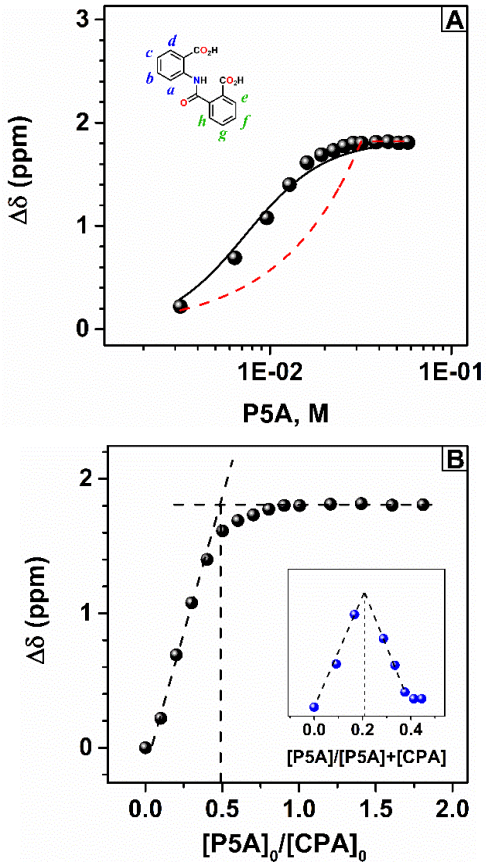

Figure 5. (A) ^{1}H NMR chemical shifts to the "H*c*" proton of CPA^{2-} in response to the increased P5A concentration, data fitting as H:G_2 (black line) and H:G (red dashed line). (B) The same chemical shifts as a function of P5A equivalent. (The inset is the Job's plot for the same data. ($[CPA^{2-}]$ = 31.87 mM; D_2O:MeOD, 1:1; 25.0 ºC; 200 MHz).

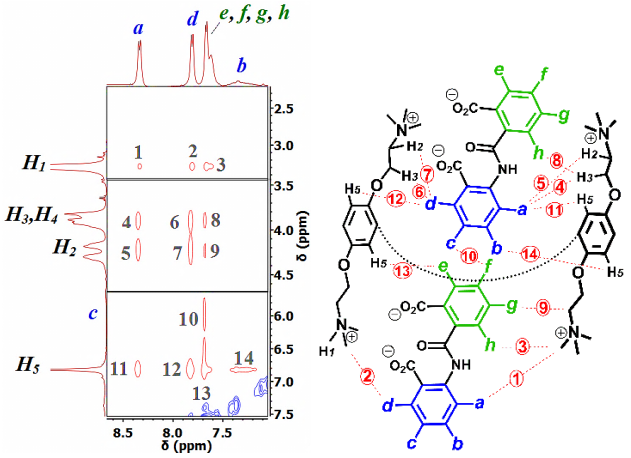

Figure 6. (Left) Partial ^{1}H ROESY spectrum of CPA^{2-} (6.4 mM) with P5A (3.2 mM) with mixing time of 225 ms (pD 7.0; D_2O:MeOD, 1:1; 25.0 ºC; 400 MHz). (Right) Map of H-H interactions deducted by the 14 cross-peaks.

Based on the cross-peaks we present a "map of H-H interactions" in the CPA^{2-}⊂P5A⊃CPA^{2-} system, with all the interactions depicted in red color (Figure 6, right). This perspective makes clear the diversity and number of possible interactions between its components, like electrostatic, cation-π, anion-π, π-π, CH-π and hydrophobic (by CPA aromatic rings). This allows us to understand the high energy stability achieved in this geometry, making this complex a reference for planning new systems. The map also elucidates the non-existence of interactions between H*b* and H*c* with the aliphatic protons of P5A, as well as the enlargement of H*b* and the splitting of H*c* (see SI) as a result of very different environments due to the asymmetry of the complex.

CONCLUSIONS

The high rate of hydrolysis of 2-carboxyphthalanilic acid (CPA) was inhibited by host-guest complexation with a pillar[5]arene functionalized with trimethylammonium groups (P5A) which deactivates intramolecular catalytic carboxyl groups. In contrast, its greater cavity analogue (P6A) showed no kinetic effects and strong evidence of external complexation inefficient in restricting the CPA carboxyl groups.

P5A promoted up to 222-fold inhibition for the CPA^{2-} decomposition. Kinetic and NMR data show hydrophobic interactions as the main driving force involved in the binding of the first CPA. Meanwhile, the binding of the second CPA strongly depends on interactions within the P5A cavity. The system showed intelligence in response to pH, with allosteric behavior and regulation by the different species of CPA. This effect was evidenced by the change of cooperativity (negative to positive), having as effector/regulator the CPA^{2-} species. Values of $K_{1:1}$ = 10^4 M^{-1} were observed for all species, while $K_{1:2}$ remained between 10^2–10^4 M^{-1}. These variations maintained K_G between 10^7–10^9 M^{-2} for CPA species.

The structural elucidation of the complex showed the antiparallel accommodation of the CPAs in the P5A cavity. In addition, the map of H-H interactions gives a good perspective of the great diversity and number of interactions between its components, making it simple to understand the high energy stabilization in the H:G_2 stoichiometry.

EXPERIMENTAL

Materials. The CPA, P5A and P6A were prepared based on the literature,[30,31] with the modifications detailed below.

Synthesis of 2-carboxyphthalanilic acid (CPA): Scheme S1 shows the two reaction steps for CPA synthesis: (step 1) condensation reaction between anthranilic acid and phthalic anhydride followed by the (step 2) opening of the imide to amide, both described below:

(Step1) In a reaction flask, was added glacial acetic acid (6.0 mL), phthalic anhydride (1.481 g, 10 mmols) and anthranilic acid (1.246 g, 9.09 mmols). The solution was refluxed for 12 h. After cooling, the reaction mixture was poured on 10.0 mL water and solid formed was filtered of, washed with water and dried under vacuum. Yield 1.28 g (53 %) as a grayish solid. ^{1}H NMR (200 MHz, DMSO-D_6, TMS): δ (ppm): 13.13 (br s, 1H), 8.09–7.49 (m, 8H). $^{13}C\{^{1}H\}$ NMR (50 MHz, DMSO-D_6, residual solvent as reference): δ (ppm): 167.1, 166.1, 134.8, 133.0, 131.8, 131.5, 131.0, 130.7, 129.2, 123.5.

(Step 2) In a reaction flask, was added H_2O (6.0 mL), NaOH (179.0 mg, 4.49 mmols) and the product of step 1 (300.0 mg, 1.12 mmols). The solution was stirred for 15 h. The reaction mixture was filtered and acidified with HCl 12 M until pH 2.0. The precipitated was filtered of, washed with water and dried under vacuum. Yield 270.5 mg (84 %) as a white solid. ^{1}H NMR (200 MHz, DMSO-D_6, TMS): δ (ppm): 13.38 (br s, 2H), 11.56 (s, 1H), 8.66 (d, J = 8 Hz, 1H), 8.06 (dd, J = 8 Hz, 1H), 7.91 (dd, J = 8 Hz, 1H), 7.72–7.59 (m, 4H), 7.22 (t, 1H). $^{13}C\{^{1}H\}$ NMR (50 MHz, DMSO-D_6, residual solvent as reference): δ (ppm): 169.6, 167.6, 167.0, 141.1, 138.1, 134.2, 131.9, 131.2, 130.5, 130.2, 129.7, 127.3, 123.0, 119.9, 116.5. ESI-MS^2 (*m/z*): $[M–H^+]^-$, 284.0 Da; $[M–H^+–H_2O]^-$, 266.1 Da; $[M–H^+–H_2O–CO_2]^-$, 221.8 Da; $[M–H^+–H_2O–CO_2–CO]^-$, 195.9 Da; [anthranilic acid–H^+]$^-$, 136.1 Da.

Synthesis of P5A and P6A: Scheme S2 shows the three reaction steps for P5A and P6A syntheses: (step 1) bromination of hydroquinone, (step 2) cyclization promoted by Lewis acid and (step 3) functionalization with trimethylammonium groups.

(Step 1) In a reaction flask under argon atmosphere hydroquinone (10.0 mmol), triphenylphosphine (23.81 mmol) and dry acetonitrile (50.0 mL) were added. This reaction mixture was cooled to 0 °C and the carbon tetrabromide (23.81 mmol) was slowly added. The reaction mixture was stirred at room temperature for 4 hours. After this period, cold water (40.0 mL) was added, resulting in a white precipitate. The precipitate was collected, washed with MeOH/H_2O (3:2, 3 x 25.0 mL), recrystallized from methanol and dried under vacuum. Yield 93% as a white solid. ^{1}H NMR (200 MHz, $CDCl_3$, TMS): δ (ppm): 6.86 (s, 4H); 4.24 (t, 4H, J = 4 Hz); 3.61 (t, 4H, J = 4 Hz). $^{13}C\{^{1}H\}$ NMR (50 MHz, $CDCl_3$, residual solvent as reference): δ (ppm): 152.9; 116.2; 68.8; 29.4.

(Step 2, for P5A) In a solution of brominated hydroquinone in CH_2Cl_2 (230 mL), paraformaldehyde (30.87 mmol) and boron trifluoride diethyl etherate (33.86 mmol) were added under argon atmosphere. The resulting mixture was stirred during 2 h at room temperature. After this time, the reaction mixture was washed with water, saturated sodium bicarbonate solution and brine. The organic layer was dried over $MgSO_4$ and the solvent was removed by vacuum. The residue was

purified by column chromatography (CH_2Cl_2:hexane) yielding 70 % of brominated pillar[5]arene as a white solid. ^{1}H NMR (200 MHz, $CDCl_3$, TMS): δ (ppm): 6.91 (s, 10H); 4.23 (t, 20H, J = 4 Hz); 3.84 (s, 10H); 3.63 (t, 20H, J = 4 Hz). $^{13}C\{^1H\}$ NMR (50 MHz, $CDCl_3$, residual solvent as reference): δ (ppm): 149.8; 129.2; 116.2; 69.1; 30.9; 29.5.

(Step 2, for P6A) In a solution of brominated hydroquinone in $CHCl_3$ (90 mL), paraformaldehyde (30.87 mmol) and $FeCl_3$ (1.24 mmol) were added under argon atmosphere. The resulting mixture was stirred during 72 h at 45 ºC. After this time, the reaction mixture was washed with water, saturated sodium bicarbonate solution and brine. The organic layer was dried over $MgSO_4$ and the solvent was removed by vacuum. The residue was purified by column chromatography (CH_2Cl_2:hexane) yielding 30 % of brominated pillar[6]arene as a pale yellow solid. ^{1}H and $^{13}C\{^1H\}$ NMR chemical shifts similar to brominated pillar[5]arene.

(Step 3) In a solution of brominated pillararene (1.19 mmol) in ethanol (100.0 mL) was added trimethylamine (48.11 mmol). The reaction mixture was refluxed overnight. After this time, the precipitate was collected, washed with EtOH and dried under vacuum. Yield 95% to P5A (white solid) and 91 % to P6A (pale yellow solid). ^{1}H NMR (500 MHz, D_2O, TMSP): δ (ppm): 6.86 (s, 1H), 4.37 (s, 2H), 3.85 (s, 1H), 3.72 (s, 2H), 3.14 (s, 9H). $^{13}C\{^1H\}$ NMR (126 MHz, D_2O, TMSP): δ(ppm): 149.4, 130.0, 116.5, 65.0, 63.5, 54.1, 29.5. HRMS/ESI-TOF (m/z) for P5A: $[P5A–3Br^-]^{3+}$ ($C_{85}H_{150}N_{10}O_{10}Br_7$), calculated 677.1917, found 677.1919; $[P5A–2Br^-]^{2+}$ ($C_{85}H_{150}N_{10}O_{10}Br_8$), calculated 1055.7472, found 1055.7473. HRMS/ESI-TOF (m/z) for P6A: $[P6A–3Br^-]^{3+}$ ($C_{102}H_{180}N_{12}O_{12}Br_9$), calculated 828.5472, found 828.5474; $[P6A–2Br^-]^{2+}$ ($C_{102}H_{180}N_{12}O_{12}Br_{10}$), calculated 1282.7799, found 1282.7795.

Kinetics. Reactions were followed with an UV-Vis spectrophotometer Cary 50 equipped with Peltier temperature controller set to 25.0 ºC. Reactions were started by adding 20 µL of the CPA solution (0.01 M, in methanol) to 2.0 mL of buffer solution in quartz cuvettes, in the presence of the P5A or P6A. All observed rate constants (k_{obs}) were measured observing the appearance of the anthranilic acid at 330-350 nm.

ESI-MS. The samples were injected directly to a mass spectrometry system consisting of a hybrid triple quadrupole/linear ion trap mass spectrometer Q trap 3200 (Applied Biosystems/MDS Sciex, Concord, Canada). The experiments were performed using the Turbo Ion Spray™ source (electrospray ionization–ESI, Applied Biosystems/MDS Sciex, Concord, Canada) in positive ion mode. Samples were infused continuously at 10 µL/min with a syringe pump. The capillary needle voltage was maintained at 5.5 kV. The MS/MS parameters were curtain gas, 10 psi; ion spray interface, 0.0 ºC; GS1, 18.0 psi; GS2, 0.0 psi; and collision gas, medium.

NMR. The NMR analyses were performed using Bruker AC 200 and 400 MHz spectrometers. To ^{1}H NMR titration, in the NMR tube containing the CPA solution (D_2O:MeOD, 1:1; pD 7.0; Bis-Tris methane or propane 0.01 M; TMSP) solid fractions of the pillararenes were added and after its total solubilization the spectra were collected. Mixing time of 225 ms was used to ^{1}H ROESY.

ASSOCIATED CONTENT

Supporting Information

The Supporting Information is available free of charge on the ACS Publications website.

Synthetic schemes; NMR spectra; HRMS spectra; Product characterization; Kinetic data; NMR experiments and treatment of the data (kinetic and NMR) (PDF).

AUTHOR INFORMATION

Corresponding Authors

*eduardoifg@hotmail.com
*ricardo.affeldt@ufsc.br

ORCID

Eduardo V. Silveira: 0000-0002-5020-1295
Vanessa Nascimento: 0000-0001-9413-7638
Eduardo H. Wanderlind: 0000-0002-0534-5898
Ricardo F. Affeldt: 0000-0003-0672-8396
Gustavo A. Micke: 0000-0002-5518-624X
Luis Garcia-Rio: 0000-0003-2802-8921
Faruk Nome: 0000-0001-8864-6807

Author Contributions

All authors have given approval to the final version of the manuscript.

Notes

The authors declare no competing financial interests.
¶ Dr. Faruk Nome passed away on 24/09/2018.

ACKNOWLEDGMENT

We dedicate this work on the memory of Professor Faruk Nome who passed away (September 24, 2018) during the preparation of this paper. His professional and personal efforts have made this possible. We thank Brazilian funding agencies CNPq, CAPES and FAPESC and Central de Análises (UFSC) for NMR analysis and CEBIME (UFSC) for HRMS/ESI-TOF analysis. RFA thanks CNPq/INCT-Catálise for financial support (grant 465454/2017-3). LGR thanks Ministerio de Economía y Competitividad of Spain (CTQ2017-84354-P), Xunta de Galicia (GR 2007/085; IN607C 2016/03) and Centro singular de investigación de Galicia accreditation (2016-2019, ED431G/09) and the European Union (European Regional Development Fund-ERDF).

REFERENCES

(1) Ogoshi, T.; Kanai, S.; Fujinami, S.; Yamagishi, T. A.; Nakamoto, Y. Para-Bridged Symmetrical Pillar[5]Arenes: Their Lewis Acid Catalyzed Synthesis and Host-Guest Property. *J. Am. Chem. Soc.* **2008**, *130* (15), 5022–5023.

(2) Nierengarten, I.; Guerra, S.; Holler, M.; Nierengarten, J. F.; Deschenaux, R. Building Liquid Crystals from the 5-Fold Symmetrical Pillar[5]Arene Core. *Chem. Commun.* **2012**, *48* (65), 8072–8074.

(3) Pan, S.; Ni, M.; Mu, B.; Li, Q.; Hu, X. Y.; Lin, C.; Chen, D.; Wang, L. Well-Defined Pillararene-Based Azobenzene Liquid Crystalline Photoresponsive Materials and Their Thin Films with Photomodulated Surfaces. *Adv. Funct. Mater.* **2015**, *25* (23), 3571–3580.

(4) Yu, G.; Ma, Y.; Han, C.; Yao, Y.; Tang, G.; Mao, Z.; Gao, C.; Huang, F. A Sugar-Functionalized Amphiphilic Pillar[5]Arene: Synthesis, Self-Assembly in Water, and Application in Bacterial Cell Agglutination. *J. Am. Chem. Soc.* **2013**, *135* (28), 10310–10313.

(5) Joseph, R.; Naugolny, A.; Feldman, M.; Herzog, I. M.; Fridman, M.; Cohen, Y. Cationic Pillararenes Potently Inhibit Biofilm

Formation without Affecting Bacterial Growth and Viability. *J. Am. Chem. Soc.* **2016**, *138* (3), 754–757.

(6) Wanderlind, E. H.; Liz, D. G.; Gerola, A. P.; Affeldt, R. F.; Nascimento, V.; Bretanha, L. C.; Montecinos, R.; Garcia-Rio, L.; Fiedler, H. D.; Nome, F. Imidazole-Functionalized Pillar[5]Arenes: Highly Reactive and Selective Supramolecular Artificial Enzymes. *ACS Catal.* **2018**, *8* (4), 3343–3347.

(7) Liz, D. G.; Manfredi, A. M.; Medeiros, M.; Montecinos, R.; Gómez-González, B.; Garcia-Rio, L.; Nome, F. Supramolecular Phosphate Transfer Catalysis by Pillar[5]Arene. *Chem. Commun.* **2016**, *52* (15), 3167–3170.

(8) Mako, T. L.; Racicot, J. M.; Levine, M. Supramolecular Luminescent Sensors. *Chem. Rev.* **2019**, *119* (1), 322–477.

(9) Li, H.; Chen, D.-X.; Sun, Y.-L.; Zheng, Y. B.; Tan, L.-L.; Weiss, P. S.; Yang, Y.-W. Viologen-Mediated Assembly of and Sensing with Carboxylatopillar[5]Arene-Modified Gold Nanoparticles. *J. Am. Chem. Soc.* **2013**, *135* (4), 1570–1576.

(10) Galan, A.; Ballester, P. Stabilization of Reactive Species by Supramolecular Encapsulation. *Chem. Soc. Rev.* **2016**, *45* (6), 1720–1737.

(11) Cram, D. J.; Tanner, M. E.; Thomas, R. The Taming of Cyclobutadiene. *Angew. Chemie Int. Ed. English* **1991**, *30* (8), 1024–1027.

(12) Brumaghim, J. L.; Michels, M.; Pagliero, D.; Raymond, K. N. Encapsulation and Stabilization of Reactive Aromatic Diazonium Ions and the Tropylium Ion within a Supramolecular Host. *European J. Org. Chem.* **2004**, No. 24, 5115–5118.

(13) Cullen, W.; Metherell, A. J.; Wragg, A. B.; Taylor, C. G. P.; Williams, N. H.; Ward, M. D. Catalysis in a Cationic Coordination Cage Using a Cavity-Bound Guest and Surface-Bound Anions: Inhibition, Activation, and Autocatalysis. *J. Am. Chem. Soc.* **2018,** *140* (8), 2821–2828.

(14) Hua, B.; Zhou, J.; Yu, G. Hydrophobic Interactions in the Pillar[5]Arene-Based Host-Guest Complexation and Their Application in the Inhibition of Acetylcholine Hydrolysis. *Tetrahedron Lett.* **2015**, *56* (8), 986–989.

(15) Yu, G.; Zhou, J.; Shen, J.; Tang, G.; Huang, F. Cationic Pillar[6]arene/ATP Host–guest Recognition: Selectivity, Inhibition of ATP Hydrolysis, and Application in Multidrug Resistance Treatment. *Chem. Sci.* **2016**, *7*, 4073–4078.

(16) Morawetz, H.; Shafer, J. Intramolecular Bifunctional Catalysis of Amide Hydrolysis. *J. Am. Chem. Soc.* **1962,** *84* (19), 3783–3784.

(17) Bjelic, S.; Åqvist, J. Catalysis and Linear Free Energy Relationships in Aspartic Proteases. *Biochemistry* **2006**, *45* (25), 7709–7723.

(18) Kirby, A. J.; Williams, N. H. Efficient Intramolecular General Acid Catalysis of Vinyl Ether Hydrolysis by the Neighbouring Carboxylic Acid Group. *J. Chem. Soc. Chem. Commun.* **1991**, No. 22, 1643–1644.

(19) Soleimani-Amiri, S.; Vessally, E.; Babazadeh, M.; Hosseinian, A.; Edjlali, L. Intramolecular Cyclization of N-Allyl Propiolamides: A Facile Synthetic Route to Highly Substituted γ-Lactams (a Review). *RSC Adv.* **2017**, *7* (45), 28407–28418.

(20) Webber, M. J.; Langer, R. Drug Delivery by Supramolecular Design. *Chem. Soc. Rev.* **2017**, *46* (21), 6600–6620.

(21) Basílio, N.; Pischel, U. Drug Delivery by Controlling a Supramolecular Host–Guest Assembly with a Reversible Photoswitch. *Chem. - A Eur. J.* **2016**, *22* (43), 15208–15211.

(22) Choi, J. H.; Laurent, A. H.; Hilser, V. J.; Ostermeier, M. Design of Protein Switches Based on an Ensemble Model of Allostery. *Nat. Commun.* **2015**, *6*, 1–9.

(23) Maurer, D.; Lohkamp, B.; Krumpel, M.; Widersten, M.; Dobritzsch, D. Crystal Structure and PH-Dependent Allosteric Regulation of Human β-Ureidopropionase, an Enzyme Involved in Anticancer Drug Metabolism. *Biochem. J.* **2018**, *475* (14), 2395–2416.

(24) Pastra-Landis, S. C.; Evans, D. R.; Lipscomb, W. N.; Lipscomb, N. The Effect of PH on the Cooperative Behavior of Aspartate Transcarbamylase from Escherichia Coli*. *J. Biol. Chem.* **1977**, 4624–4630.

(25) Jiang, M.; Li, M.; Liu, L.; Xiang, M.; Zhu, L. Macromolecular Aggregation: Complexation Due to Hydrogen Bonding and Hydrophobic Association. *Macromol. Symp.* **1997**, *124*, 135–146.

(26) Menger, F. M. Enzyme Reactivity from an Organic Perspective. *Acc. Chem. Res.* **1993**, *26* (4), 206–212.

(27) Gómez, B.; Francisco, V.; Fernández-Nieto, F.; Garcia-Rio, L.; Martín-Pastor, M.; Paleo, M. R.; Sardina, F. J. Host-Guest Chemistry of a Water-Soluble Pillar[5]Arene: Evidence for an Ionic-Exchange Recognition Process and Different Complexation Modes. *Chem. - A Eur. J.* **2014**, *20* (38), 12123–12132.

(28) Dodziuk, H.; Nowinski, K. S.; Kozminski, W.; Dolgonos, G. On the Impossibility of Determination of Stepwise Binding Constants for the 1:2 Complex of (+)-Camphor with α-Cyclodextrin. *Org. Biomol. Chem.* **2003**, *1* (3), 581–584.

(29) Ulatowski, F.; Dabrowa, K.; Bałakier, T.; Jurczak, J. Recognizing the Limited Applicability of Job Plots in Studying Host-Guest Interactions in Supramolecular Chemistry. *J. Org. Chem.* **2016**, *81* (5), 1746–1756.

(30) Wiklund, P.; Romero, I.; Bergman, J. Products from Dehydration of Dicarboxylic Acids Derived from Anthranilic Acid. *Org. Biomol. Chem.* **2003**, *1* (19), 3396–3403.

(31) Xue, M.; Yang, Y.; Chi, X.; Zhang, Z.; Huang, F. Pillararenes, A New Class of Macrocycles for Supramolecular Chemistry. *Acc. Chem. Res.* **2012**, *45* (8), 1294–1308.

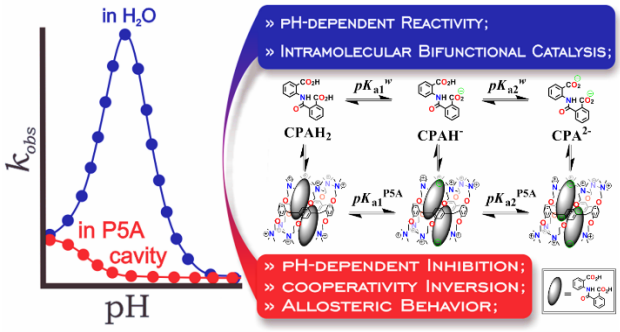
in H_2O
k_{obs}
in P5A cavity
pH
» pH-dependent Reactivity;
» Intramolecular Bifunctional Catalysis;
pK_{a1}^{W}
pK_{a2}^{W}
$CPAH_2$
$CPAH^-$
CPA^{2-}
pK_{a1}^{P5A}
pK_{a2}^{P5A}
» pH-dependent Inhibition;
» Cooperativity Inversion;
» Allosteric Behavior;